Research Article

Chaojun Gao, Daiqin Liu*, Jie Li, Chunyan Song, Gulizinati Yideresi, and Ailixiati Yushan

Deep fault sliding rates for Ka-Ping block of Xinjiang based on repeating earthquakes

https://doi.org/10.1515/geo-2022-0610
received November 11, 2023; accepted January 29, 2024

Abstract: The seismically active Ka-Ping Block within Xinjiang, China, represents a zone of potential earthquake hazards, and existing surface measurements cannot fully reflect the area's sub-surface slip rates. To determine these slip rates and characterize the level of hazard that the study area may face in future years, using a cross-correlation of waveforms, we identified 432 repeat sequences along large faults (F1–F5) in the Ka-Ping Block between September 2009 and April 2022 and computed the annual slip rate for every sequence with the empirical relationship of the moment and the seismic magnitude. Spatial distribution images and temporal evolution characteristics of deep deformation in fault zones were constructed. We obtained five asperities in the Ka-Ping Block, the western portion of the PiQiang fault (F4) had a larger yearly slide rate than its eastern portion, and the southwest and eastern areas of the KEP station show an elevated risk of seismic activity within the next two years.

Keywords: repeat sequences, slip rates, deep deformation, risk of seismic

*** Corresponding author: Daiqin Liu**, Xinjiang Pamir Intracontinental Subduction National Field Observation and Research Station, Urumqi 830011, Xinjiang, China; Earthquake Agency of the Xinjiang Uygur Autonomous Region, No. 338 Kexue Second Street, Urumqi 830011, Xinjiang, China, e-mail: xjdzjldq@126.com
Chaojun Gao, Chunyan Song: Xinjiang Pamir Intracontinental Subduction National Field Observation and Research Station, Urumqi 830011, Xinjiang, China; Earthquake Agency of the Xinjiang Uygur Autonomous Region, No. 338 Kexue Second Street, Urumqi 830011, Xinjiang, China
Jie Li: Xinjiang Pamir Intracontinental Subduction National Field Observation and Research Station, Urumqi 830011, Xinjiang, China; Earthquake Agency of the Xinjiang Uygur Autonomous Region, No. 338 Kexue Second Street, Urumqi 830011, Xinjiang, China; Urumqi Institute of Central Asia Earthquake, China Earthquake Administration, Urumqi 830011, Xinjiang, China
Gulizinati Yideresi: Earthquake Agency of the Xinjiang Uygur Autonomous Region, No. 338 Kexue Second Street, Urumqi 830011, Xinjiang, China
Ailixiati Yushan: Earthquake Agency of the Xinjiang Uygur Autonomous Region, No. 338 Kexue Second Street, Urumqi 830011, Xinjiang, China

1 Introduction

Generally, earthquakes with large magnitude caused significant destruction according to the epicenter area [1]. If we know the potential seismic risk of the region in the next 3–5 years, we can reduce a lot of unnecessary losses in urban construction and economic development, which is very important in our lives.

The Ka-Ping Block, which is situated on the west of Xinjiang's southern Tien-Shan, China, contains four large faults, is one of the strongest areas for crustal movement, and has been impacted by several earthquakes causing disaster in Xinjiang since 1900 (Figure 1). Some experts carried out a lot of research on this region. The detailed information on each fault zone in the block has been obtained through a large number of field geological investigations [2]. Yang found that the crust shortening on the west side is greater than that on the east side, and the rate of shortening of the crust is 15.4–17.3 mm/year [3]. The paleo-earthquakes and fault slip rates in this area are studied by means of trench excavation, dating, and scarp survey [4]. GPS measurements indicated that the active faults in this region move northward relative to Eurasia at a rate of 10–20 mm per year (Figure 1) [5]. However, it is difficult to determine how fast the ground is moving deep beneath before an earthquake simply by looking at the surface [6].

Repeating earthquakes are a group of earthquakes that happen in the same place repeatedly. Geller et al. [7] studied four similar earthquakes on the San Andres Fault in Central California, and the theoretical background is that earthquakes occur when stress is repeatedly released at the same point, known as an asperity or stress concentration, along the fault surface. Identifying these asperities can help in understanding the series of events that lead to the occurrence of a larger earthquake. Nadeau et al. [8] found that the repeated earthquake is a repeated rupture

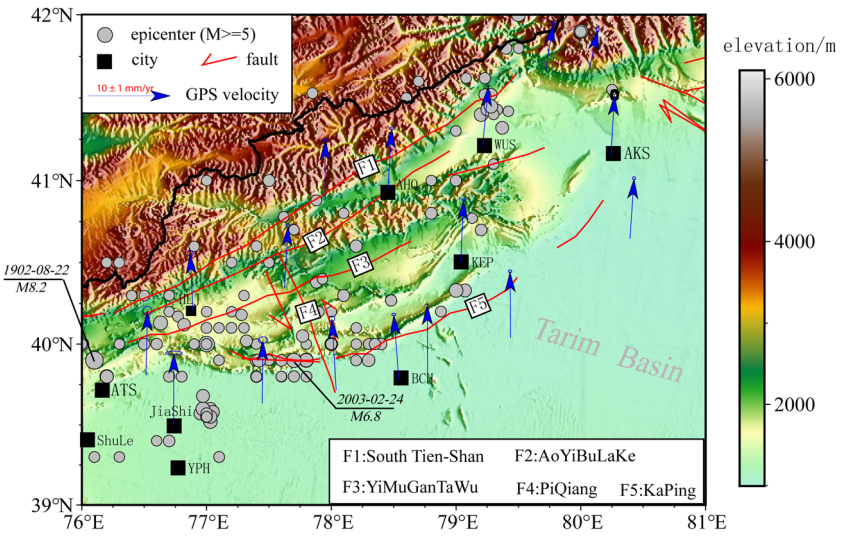

Figure 1: Spatial distribution of the faults and the epicenter of events ($M_S \geq 5.0$) with the GPS velocity field (data are from the China Earthquake Networks Center, between 1999 and 2020) in the study area.

of a strong asperity surrounded by a stable slip area, and the rupture is completed under stable regional stress loading. It is very important to study the deep deformation of a fault for analyzing its seismic risk. The discovery of repeated earthquakes provides a new method and idea for obtaining slip information of faults with different seismic depths.

As a natural"Underground creep meter," the repeat earthquake has the advantage of "*In-situ* observation" of deep deformation of faults that cannot be replaced by surface observation data, the slip rate of the fault creep zone can be studied by the size and periodicity of repeated earthquakes, and observing the rupture rate of faults has become a critical method for gaining insights into the healing process of faults in the earth. This approach enables us to understand the real-life implications of the laboratory findings on the behavior of faults and friction [9,10]. We can use this method to study behavioral aspects along a certain fault zone in Taiwan, along the part of the Longitudinal Valley fault which is between the Chi-shang and Hua-lien [11]. This method is also used to compute slip rates along faults and speculate on asperities within large co-seismic slips [12–16].

Simultaneously, various seismic activities occurred near the faults in Ka-Ping Block, and different fault deformation rates from repeating earthquakes in the area mean different earthquake hazard risks in this study area.

To improve this hazard assessment, we analyze the waveform recorded by the Xinjiang Seismic Station (XJSS) and search for repeating earthquakes along the five large faults, to compute the deep sliding rates along these faults, and we can deduce the asperities in spatial distribution. This method is similar to Kate Huihsuan Chen's, in which she used repeating earthquake sequences to identify the asperities [11]. Moreover, for repeating earthquake sequences, we can use the accumulated release of energy as the temporal distributions, to determine the future seismic potential risk over a long period. This method in temporal is similar to Lile's, in which she computed the Cumulative slip for the 15 repeating earthquake sequences along the Longmenshan fault zone [14].

This article focused on the Ka-Ping Block mentioned article used the asperity and the accelerated release of accumulated energy to estimate where and when the risk of a large seismic hazard may occur. In addition, the method in spatial and temporal distributions mentioned above makes a significant contribution to the literature and fills this research gap.

2 Data and methods

2.1 Five faults in the Ka-Ping block

The Ka-Ping Block is located in the western segment of South Tien-Shan, northwest Xinjiang, China. The block spans from Wushi County of the Aksu Region to Atushi City of the Kizilsu Kergez Autonomous Prefecture Region, a big rectangle about 400 km long and 200 km wide (Figure 1). Several strong earthquakes have happened in this area, such as the Atushi approximately 8.2 magnitude (M)

earthquake in 1902, the Jiashi-Bachu M6.8 earthquake in 2003, and more than 30 earthquakes with M > 6 that occurred between 1902 and 2003 [17].

There are numerous faults located in the above-mentioned block, four of which are large and widely known. These include the South Tien-Shan fault in the north (F1), traveling southward through the AoYiBuLaKe (F2), YiMuGanTaWu (F3), and PiQiang faults (F4), and ending at the Ka-Ping fault (F5). The respective lengths of the five faults are 325, 235, 280, 70, and 400 km.

2.2 Seismic data

For the above area, we found a total of 19,442 seismic events from the bulletins of the XJSS between September 2009 and April 2022, amounting to 110 GB of data with wave-forms recorded at nine stations along the four faults in the Ka-Ping Block (39.50–42.50°N and 76.00–81.50°E). There were 4,743, 5,388, 5,142, and 2,664 events within 20 km of the above five faults (F1, F2, F3, and F5, respectively).

For these events, the magnitude is from 0.0 to 4.9 on the Richter magnitude scale, the sampling rate was 100 Hz, and the number of surrounding stations was nine (i.e., AHQ, ALR, AKS, BCH, BPM, WUS, SMY, XKR, and YPH). Only three stations were located inside the events along the faults; the other six stations were located in the vicinity of the events along the faults (Figure 2).

2.3 Similar earthquake clusters

In our study, the cross-correlation method was used to obtain similar waveforms for the same station. However, when identifying and analyzing "similar earthquakes," two empirical concepts are often considered. One is the assumption that the cross-correlation coefficient (CCC) is exponentially dependent on the separation distance of the two "similarity" [18,19], and the other is a 0.5–5.0 Hz band pass filter should be used in identifying "doublets" or "multi-lets" [20,21]. In fact, we can use a 1–5 Hz relatively stable filter band in pre-processing for calculating the cross-correlation coefficient of every two events, since the variation of CCC is complicated when the frequency is above 5 Hz or below 1 Hz [22].

During the process of calculating the CCC, we select a complete waveform consisting of P, S, and the coda phase as the waveform begins 4 s (i.e., 4 seconds) before the time of P arrives and ends at four times with the time of S–P travel time difference. For an event of a pair, the seismic record of its "repeater" is slipped if its waveform length is 4 s shorter than the length of the entire waveform and slides in steps of one sample from the starting point (4 s before P arrives), taking the peak absolute of correlation coefficient as the "final" cross-correlation coefficient (CCC).

In total, for the 19,442 events mentioned earlier, we computed 24 million correlation measurements and obtained 45,312 similar event pairs, which satisfied the condition that at least one station had a CCC > 0.8. If the same pair had a

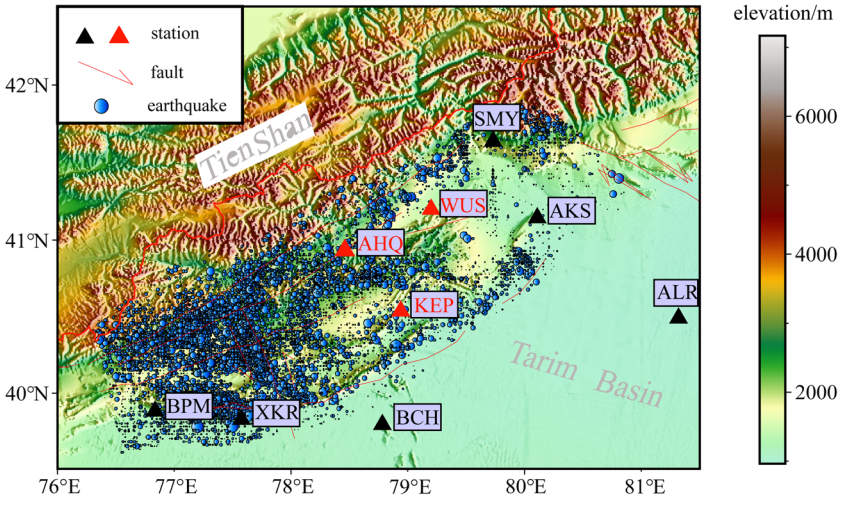

Figure 2: Spatial distribution of seismic events ($0 \le M_s \le 4.9$) and the monitoring stations within the study area. Stations located within event zones are designated with red triangles, and those outside of the event zones are designated with black triangles.

different CCC because of different stations, we computed the mean value as the CCC of the event pair and ultimately obtained 37,986 similar event pairs.

Classing the pairs into similar event cluster if two similar event pairs share a common event (i.e., A, B, and C appear to belong to a similar event cluster, if A and B represent a similar event pair, and simultaneously A and C represent another similar event pair), we identified 1,245 similar event clusters. These clusters included 730 doublets which consist of two events, and 515 multi-lets which consist of no less than three events. The number of events in the above clusters was 8,280, and the magnitudes of these events ranged from M_s 0.1 to 4.9 (Figure 3a).

To see how discrete each similar earthquake is in magnitude, recurrence interval, duration (the lifetime of a cluster or sequence), and so on, we use the coefficient of variation (COV for short, that is, the standard deviation divided by the mean) to represent the statistic of the degree of data dispersion [23]. Generally, the greater the value of COV, the greater the degree of dispersion for the data. When COV is equal to 0 indicates perfect periodicity, which means that all the data in the data set are the same and there is no dispersion. Otherwise, it indicates that the data have a certain degree of dispersion. Especially, when COV is less than 1, it means the data have a quasi-periodic feature. When COV is equal to 1, it indicates a Poisson feature, meaning the data are unpredictable. When COV is greater than 1, it means the degree of dispersion is great, changing to temporal clustering [24].

Obviously, the events in each cluster showed higher variation in recurrence interval (Figure 3d) than in magnitude (Figure 3b). Figure 3c depicts that the recurrence intervals range from a few days to several hundred days. Figure 3d shows that more than 80 clusters have a large COV, which is between 1.4 and 1.5, exhibiting a temporal cluster feature; meanwhile, there are a lot of clusters that have a small COV, which is less than 1, which means quasi-periodic features. Figure 3e depicts that a lot of clusters persisted for a few days, meaning that they were either aftershocks or earthquake swarms. Figure 3f demonstrates that clusters with long minimum values in recurrence interval(larger than 100 days) exhibited a relatively low variation(COV < 1) and shows more quasi-periodic features.

2.4 Identification of repeating earthquake sequences

Similar clusters include both repeating events and similar aftershocks or swarm events that do not occur repeatedly and exhibit a huge difference in recurrence intervals. Consequently, accurately distinguishing repeated events from similar events is vital [25].

To identify the repeating earthquakes, we used the following criteria: first, the average CCC was larger than 0.9. This is because the larger the value CCC, the higher its repeatability in position. Second, the internal inconsistency was lower than 0.5 ms in travel time [26], which can be considered an indicator of measurement error. Third, the value of the recurrence interval was more than 100 days so the clusters owned a low COV. As shown in Figure 3f, the small recurrence interval indicates a trigger or micro-aftershock process, which occurs in the fault zone with a close location but no overlap.

Based on the above three conditions, we identified 432 repeat sequences (sequences, distinguished from the clusters in “similar clusters”) including 1,243 earthquakes, which accounted for 6.4% of the total events (19,441). In contrast, 307 double-lets and 125 multi-lets were observed (Figure 4).

2.5 Deep slip rates of sequences

For all the above 432 sequences, we used the following steps to determine the slip of every event in one sequence.

We computed the co-seismic slip of each repeating event using the following empirical relationship and relative calculate formulas (1)–(3) [8,27–29]:

$$\log\left(\frac{\Delta\sigma}{2\mu}M_0\right) = 16.1 + 1.5M_S, \tag{1}$$

$$r = \sqrt[3]{\frac{7M_0}{16\Delta\sigma}}, \tag{2}$$

$$d = \frac{M_0}{\mu\pi r^2}. \tag{3}$$

Here, M_S denotes the surface magnitude, M_0 denotes the scalar moment, and r denotes the rupture size, $\Delta\sigma$ denotes the co-seismic stress drop; we used a value of approximately 8 MPa [29], d denotes the slip value, μ denotes the shear modulus, and is usually taken as 3×10^{10} N/m^2, π designates the circumference ratio.

To obtain the annual slip, we used a linear regression of the cumulative slip for every sequence, More specifically, assuming that the sliding amount corresponding to the ith earthquake is d_i, and the sliding amount corresponding to the first earthquake is 0, the horizontal and vertical coordinates for the ith point are t_i, and the sum of the previous seismic sliding amounts $D_i = 0 + d_2 + d_3 + \cdots + d_i$. So, we can obtain the annual slip rate of the sequence using the cumulative slip D_{end} divided by the time difference (t_{end} minus t_1; Figure 5).

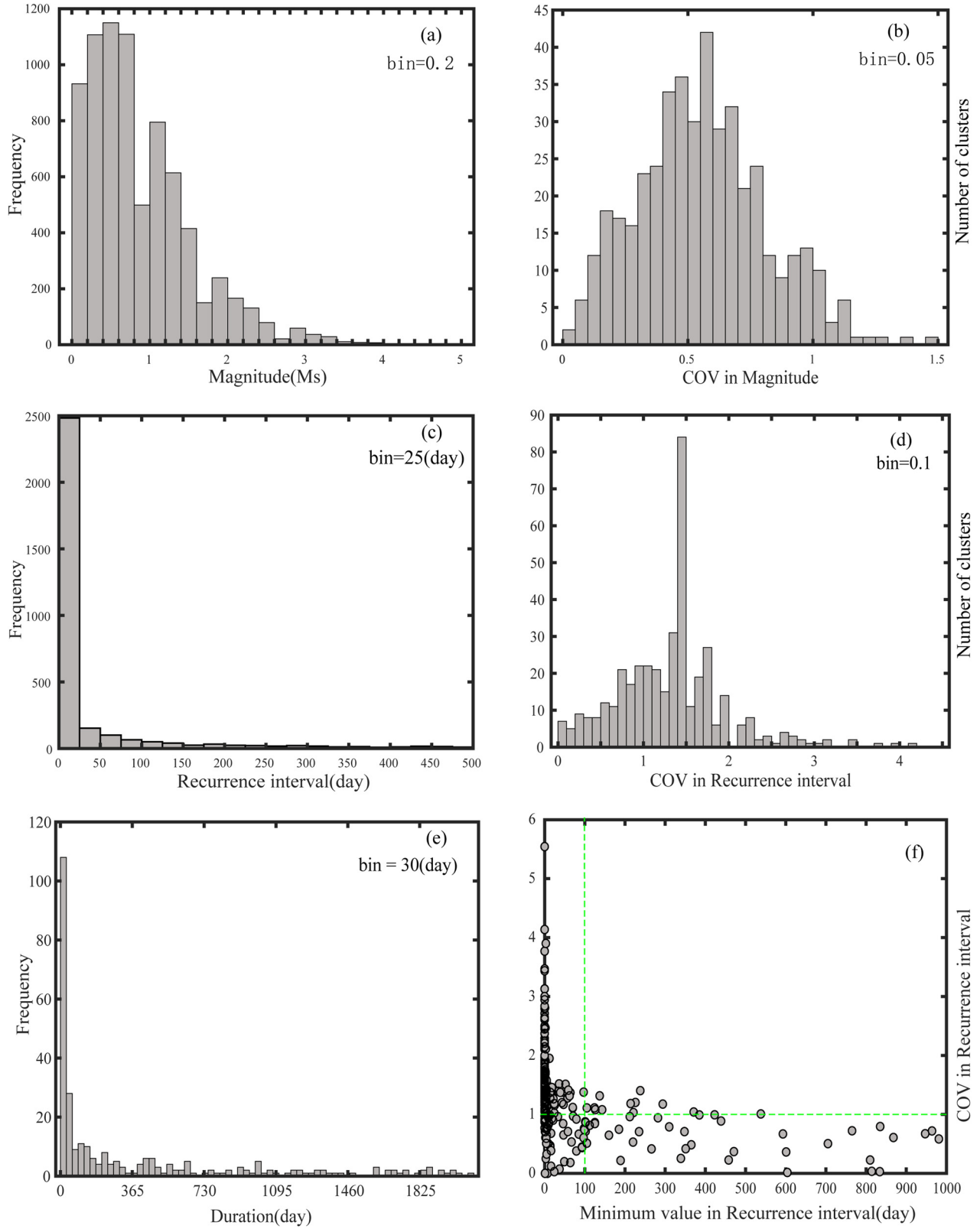

Figure 3: (a) Histogram of the magnitude distribution of similar events. (b) COV in magnitude for multi-lets clusters. (c) Histogram for recurrence intervals of multi-lets clusters. (d) COV in recurrence intervals for multi-let clusters. (e) Histogram of multi-let clusters' duration (the lifetime of every cluster). (f) COV in recurrence interval with the minimum value of every cluster. The green dashed line parallel to the *X*-axis corresponds to a COV value of 1, and the green dashed line parallel to the *Y*-axis denotes that the minimum recurrence interval is 100 days.

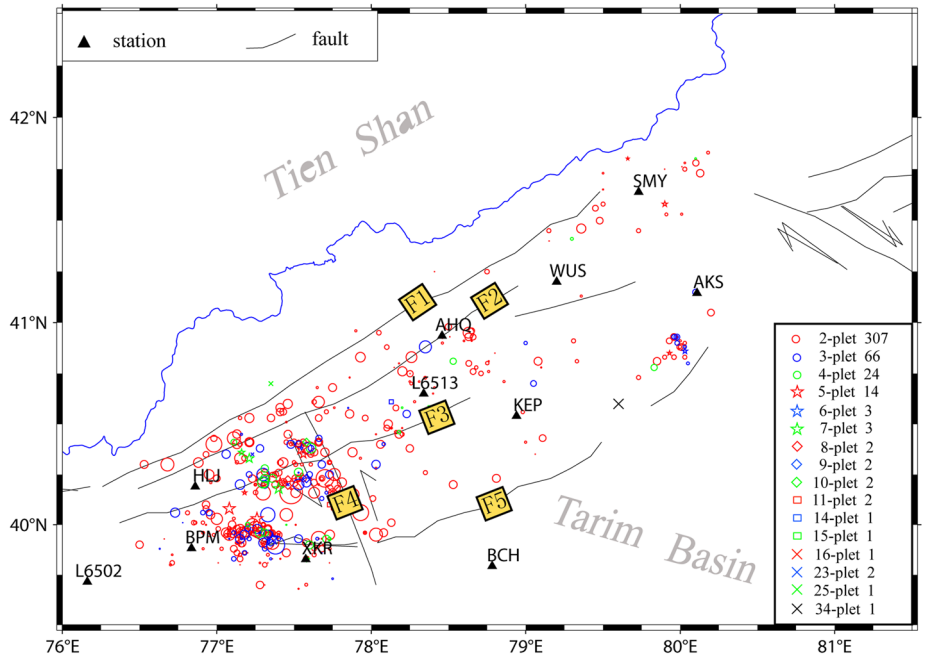

Figure 4: Spatial distribution of 432 repeat sequences. Symbol size is proportional to the magnitude of the one event from every sequence. The names of faults (F1–F5) are the same as in Figure 1.

3 Results

3.1 Spatial distribution of the repeating earthquakes

The location of an event in the XJSS directory is usually determined by the arrival time of P and S waves, the positioning method used is hypo71 or hypo2000, and the one-dimensional velocity model consists of two flat uniform layers, so that the errors in position range from a few to tens of kilometers. Consequently, it is necessary to relocate earthquakes with high precision for further analysis.

In this study, to relocate the relative locations of the entire events more effectively, we used a six-layer one-dimensional velocity model derived from CRUST1.0 (Table 1) and the double-difference method(HypoDD). The HypoDD method minimizes the residuals between the observed differential times measured for pairs of earthquakes on the same station and the theoretically calculated travel times [30]. This method does not locate each event separately but rather exports a set of positions that are most suitable for the relative propagation time of all events, especially when precise differential propagation time can be obtained by performing waveform cross-correlation.

For every sequence, using the method from Section 2.5 to compute the annual slip rate, and combining the relocation, we can plot the space distribution of the slip rate for all 432 sequences, in which the location of one solid circle means the center of one sequence and the color of one

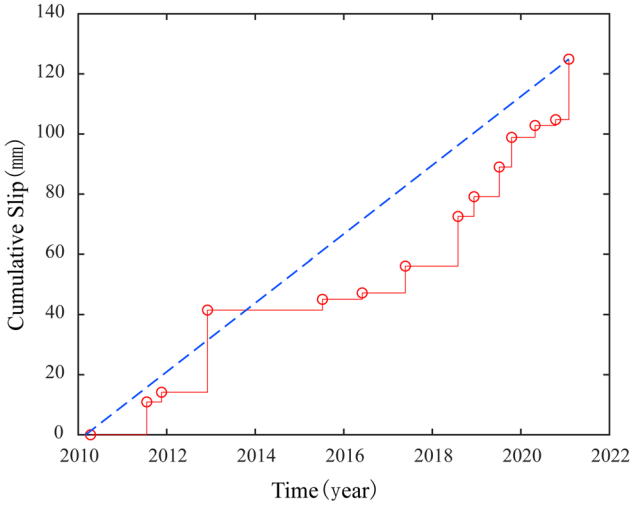

Figure 5: Schematic diagram for calculating the annual slip rate (the 14-plet sequence in chronological order).

Table 1: Six-layer one-dimensional velocity model from CRUST 1.0

Top depth (km)	0.00	5.00	10.00	20.00	35.00	50.00	75.00
Vp (km/s)	5.02	5.89	6.10	6.40	5.55	7.97	8.30
Vs (km/s)	2.90	3.40	3.53	3.70	3.21	4.61	4.80

solid circle denote the value of slip rate of one sequence (Figure 6).

Considering the impact of depth, four profiles were created along the strike of the fault zone (F1, F2, F3, and F5). The following profiles and lengths were designated: the lengths of AA′, BB′, CC′, and DD′ were 380, 380, 380, and 345 km, respectively. The corresponding widths of AA′, BB′, CC′, and DD′ were 30, 30, 30, and 40 km.

We usually combine the precise positioning results with the above sequences to identify the asperities within the profile among the spatial correspondence. The big asperity was completely locked in the inter-seismic period, the small and isolated asperities always emerge as repeat micro-earthquakes among the seismic slipping area[31–33]. Under the above assumption, the occurrence of repeated earthquakes often leads to co-seismic sliding in deep faults, and we can measure the faults' deformation in the seismogenic depths.

The profile AA′ provides insight into the depth distribution of the recurrent earthquake for the South Tien-Shan fault (F1 in Figure 7a). The maximum slip rates are found with a depth range of 12–20 km, the annual slip rate was between 0.23 mm/year at a depth of 6 km and 32.8 mm/year at 12.8 km, with a mean of 4.57 mm/year and a median of 2.0 mm/year for these sequences. Based on Figure 7a, the position of the asperity was identified from AHQ to WUS along F1, and the depth section was from 0 to 15 km.

For the AoYiBuLaKe fault (F2), we can see the depth distribution of the repeated earthquake on the profile BB' (Figure 7b). The maximum slip rates are found with a depth range of 9–17 km; the annual slip rate was between 0.24 mm/year at a depth of 5 km and 34.0 mm/year at 9 km, with a mean of 4.08 mm/year and a median of 1.45 mm/year for these sequences. Based on Figure 7b, the position of the asperity was identified from WUS to SMY along F2, and the depth section was from 0 to 20 km. If the PiQiang fault (F4) is considered the line of demarcation, the average slip rate in the west was higher than that in the east.

For the YiMuGanTaWu fault (F3), we can see the depth distribution of the repeated earthquake on the profile CC (Figure 7c). The maximum slip rates are found with a depth range of 13–15 km; the annual slip rate was between 0.25 mm/year at depth of a 7 km and 27.47 mm/year at 14.3 km, with a mean of 4.89 mm/year and a median of 2.97 mm/year for these sequences. Based on Figure 7c, the position of the asperity was identified from WUS to SMY along F3, and the depth section was from 0 to 15 km. Similar to the Aoyibulake fault (F2), if we designate the Pi-Qiang fault (F4) as the line of demarcation, the average slip rate of the west is higher than that of the east too.

For the Ka-Ping fault (F5), we can see the depth distribution of the repeated earthquake on profile DD' (Figure 7d). The maximum slip rates are found with a depth range of 13–15 km, the annual slip rate was between 0.21 mm/year

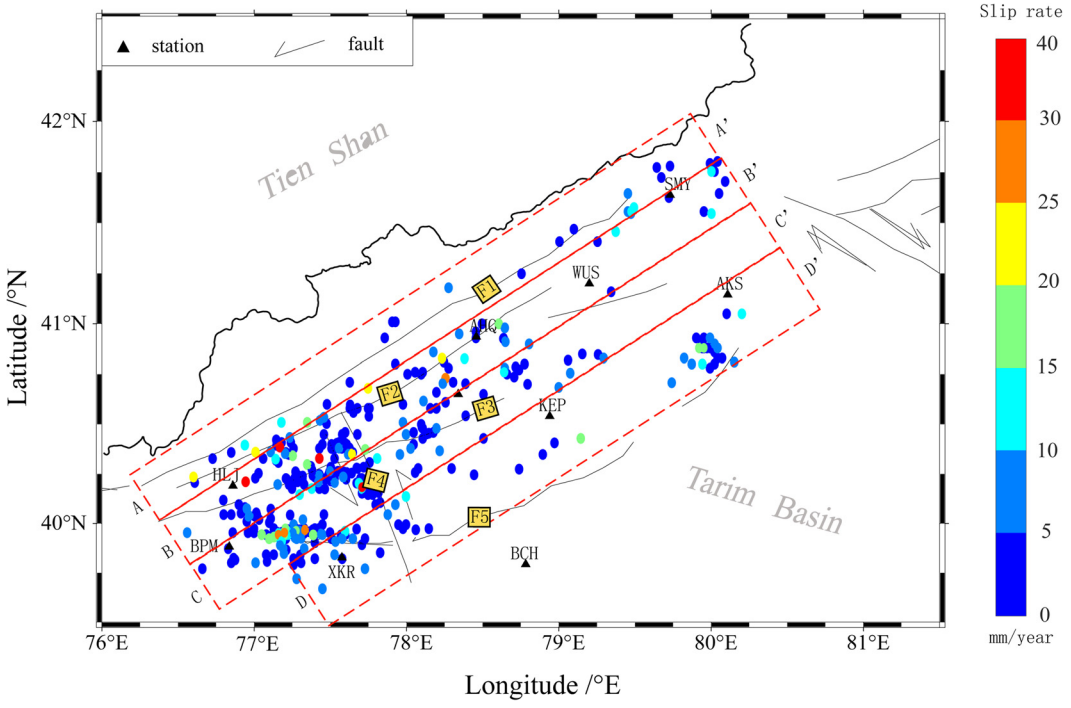

Figure 6: Spatial distribution of the 432 repeat sequences; the change in color indicates the value of the sliding rate. The names of the faults (F1–F5) correspond to those of Figure 1. The red rectangular boxes indicate the ranges of profiles AA′, BB′, CC′, and DD′.

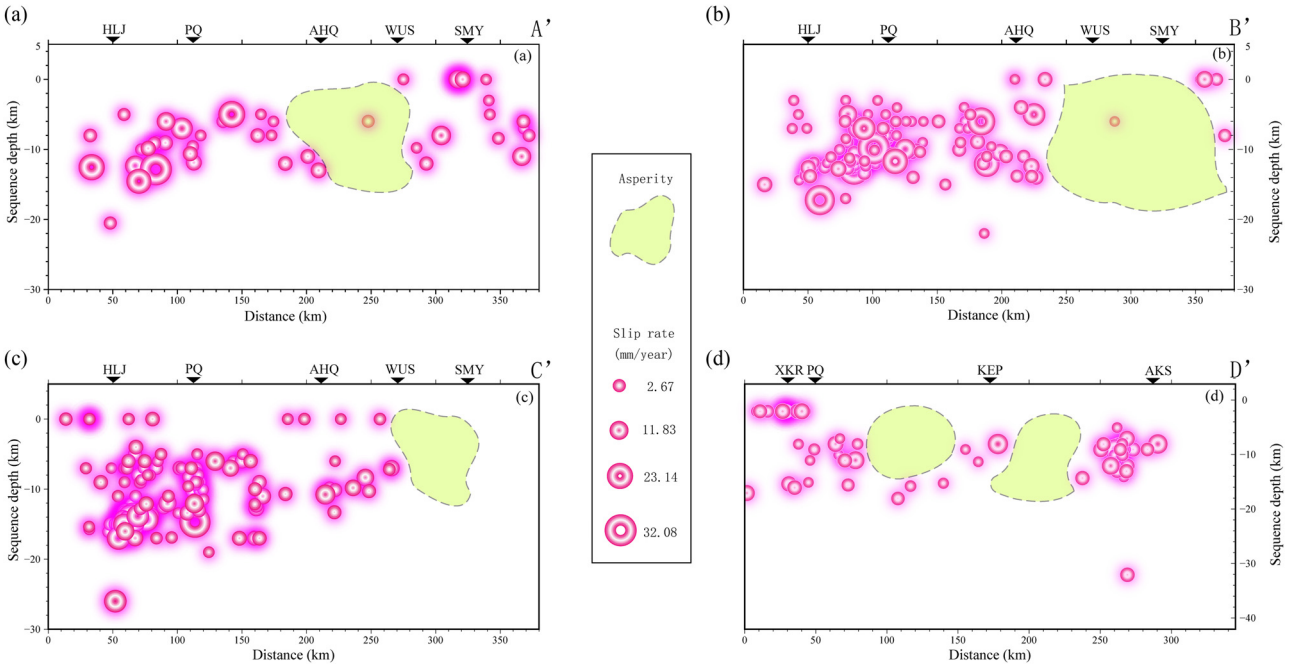

Figure 7: (a) Annual slip rate in depth under profile AA′ along the South Tien-Shan fault (F1). (b) Annual slip rate in depth under profile BB′ along the AoYiBuLaKe fault (F2). (c) Annual slip rate in depth under profile CC′ along the YiMuGanTaWu fault (F3). (d) Annual slip rate in depth under profile DD′ along the Ka-Ping fault (F5). The size of the circles is proportional to the slip rates. The light yellow areas surrounded by the dotted line are the location of asperities.

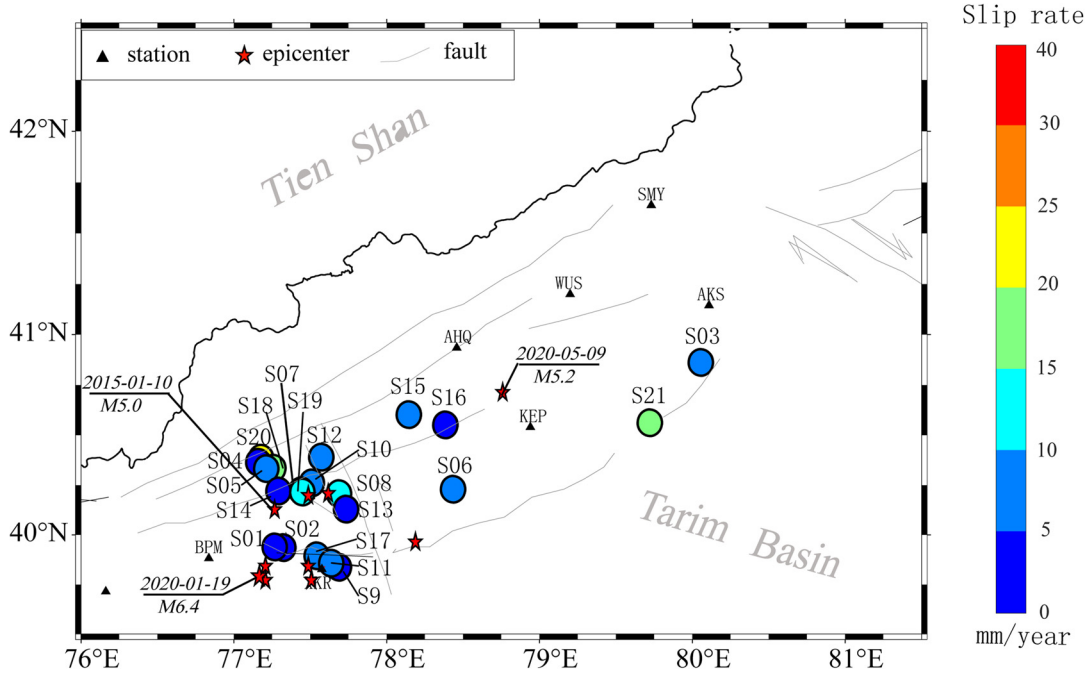

Figure 8: Spatial distribution of the 21 repeat sequences containing more than six events (solid circle) and the $M \geq 5.0$ epicenter (red star); the change in color indicates the annual sliding rate value.

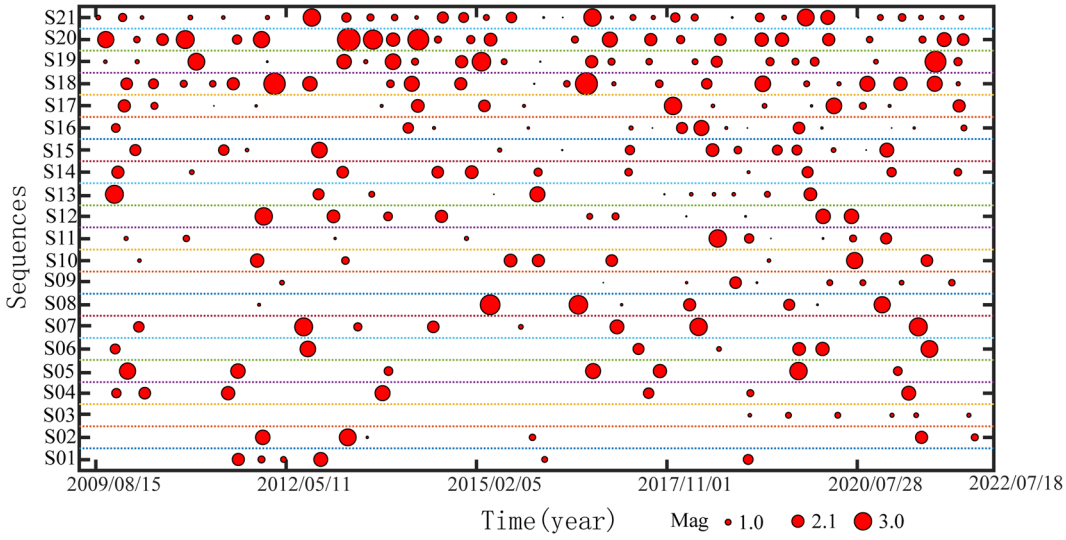

Figure 9: Occurrence times of the earthquakes in the 21 sequences. Symbol sizes are proportional to magnitudes of the earthquakes.

at a depth of 8 km and 27.5 mm/year at 14 km, with a mean of 4.59 mm/year and a median of 3.0 mm/year for these sequences. Based on Figure 7d, two positions of asperity were identified: the first is from 90 to 150 km along F5, with a depth section from 0 to 10 km; the second is from KEP station to 240 km along F5, with a depth section was from 0 to 16 km.

3.2 Temporal distribution for part of repeating earthquake sequences

We obtained 21 sequences containing more than six events in one repeating earthquake sequence. The spatial distribution is shown in Figure 8, the time-series distribution is

Table 2: Repeating earthquake sequences identified in Ka-Ping Block

Sequence	N^a	Sequence central location			M_s	D^b (days)	Cumulative slip (mm)	Slip rate (mm/year)
		Latitude (deg)	Longitude (deg)	Depth (km)				
S1	6	39.9591	77.2631	14.5	1.0–2.4	2,679	22.10	3.00
S2	6	39.9558	77.3191	14.1	0.4–2.9	3,741	33.70	3.29
S3	6	40.8600	80.0300	16.0	0.6–1.0	1,186	20.75	6.39
S4	7	40.3726	77.1562	11.2	1.2–2.6	4,162	45.78	4.01
S5	7	40.3414	77.2084	12.5	1.5–2.6	4,047	59.50	5.37
S6	7	40.2409	77.4212	11.5	0.8–2.9	4,278	64.61	5.51
S7	8	40.2334	77.4358	12.1	0.8–3.1	4,095	95.79	8.54
S8	8	40.2195	77.6806	11.1	0.3–3.4	3,274	99.80	11.13
S9	9	39.8600	77.6800	7.0	0.1–2.0	3,519	31.85	3.30
S10	9	40.2717	77.5042	10.8	0.6–2.8	4,137	58.39	5.15
S11	10	39.8800	77.6300	15.0	0.1–3.0	3,992	54.26	4.96
S12	10	40.3975	77.5656	8.3	0.3–3.0	3,087	53.37	6.31
S13	11	40.1437	77.7266	11.3	0.2–3.1	3,657	48.15	4.81
S14	11	40.2322	77.2872	12.9	0.5–2.2	4,412	50.96	4.22
S15	14	40.6052	78.1339	10.9	0.1–2.4	3,948	63.32	5.85
S16	15	40.5550	78.3712	12.2	0.1–2.6	4,527	56.13	4.53
S17	16	39.9159	77.5356	13.3	0.4–3.0	4,397	95.47	7.93
S18	23	40.3437	77.2542	11.5	0.7–2.7	4,449	236.25	19.38
S19	23	40.2272	77.4426	13.3	0.2–2.9	4,491	175.90	14.30
S20	25	40.3924	77.1746	9.6	1.1–3.9	4,587	290.86	23.14
S21	34	40.5656	79.6987	12.0	0.1–3.0	4,627	203.53	16.06

[a]Number of events in one sequence.
[b]Duration of each repeated earthquake sequence.

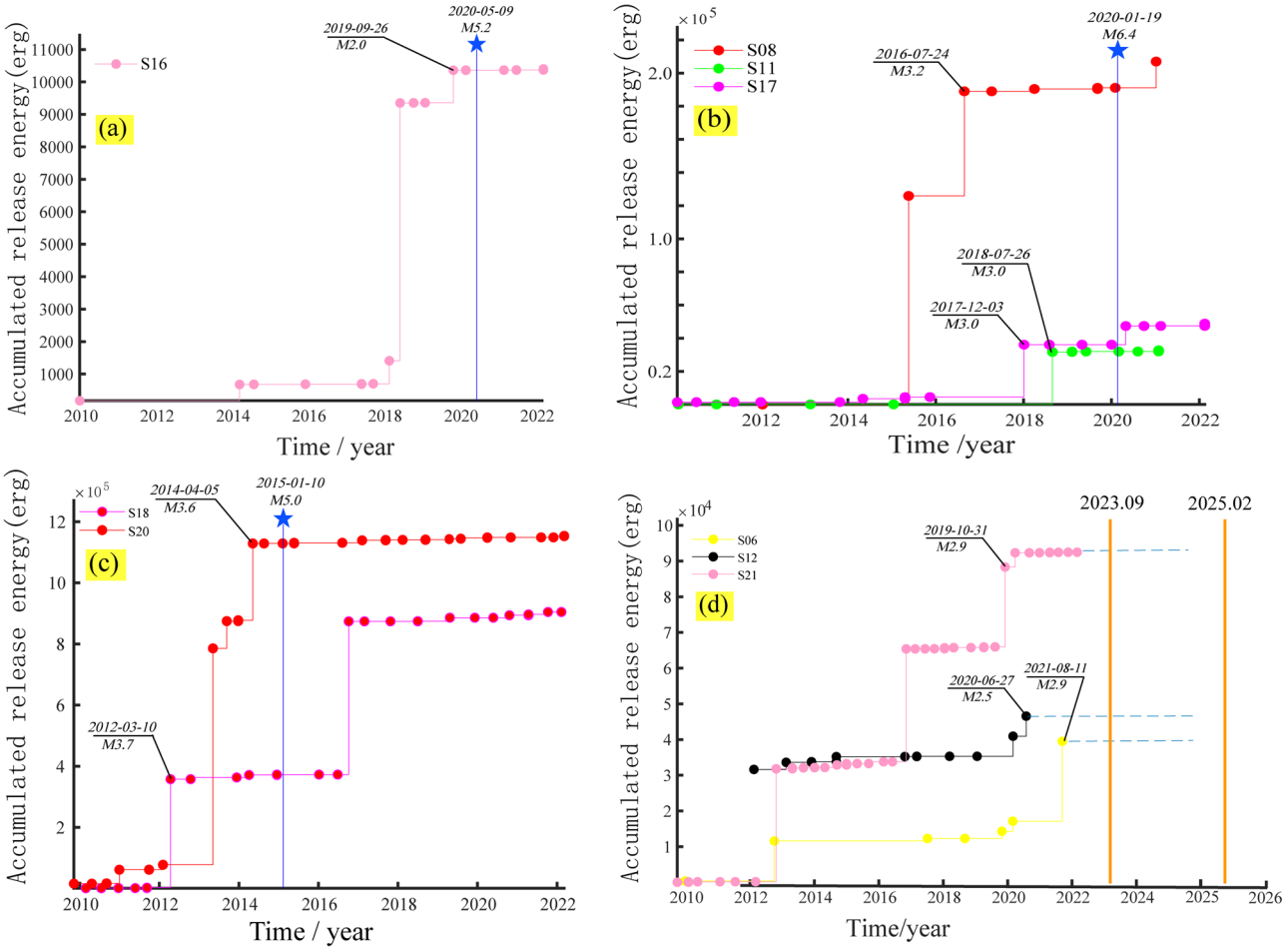

Figure 10: Horizontal and vertical coordinates of every solid circle designating the time of the earthquake and the total energy of all earthquakes before this earthquake with (a) accumulated release of energy of repeating earthquakes for S16. The blue solid vertical line is the M5.2 earthquake that occurred on May 9, 2020. (b) Accumulated release of energy of repeating earthquakes for S08, S11, and S17. The blue solid vertical line is the M6.4 earthquake that occurred on January 19, 2020. (c) Accumulated release of energy of repeating earthquakes for S18 and S20. The blue solid vertical line is the M5.0 earthquake that occurred on January 10, 2020. (d) Accumulated release of energy of repeating earthquakes for S06, S12, and S21. The left orange solid vertical line is the current time, and the right orange solid vertical line is the deadline.

shown in Figure 9, and the detailed calculation results are shown in Table 2.

Figure 8 shows five sequences (S3, S6, S15, S16, and S21) located on the eastern of the PiQiang fault (F4), and the other 16 sequences were concentrated on the western of the PiQiang fault. The annual slip rate ranged from 3 mm/year for S1 to 23.14 mm/year for S20.

Figure 9 indicates the time distribution of the above 21 sequences, and the recurrence interval of these sequences varies from a few days to several years. For example, S21

Table 3: Slip value(unit: mm) of one event rupture with different magnitude in different empirical relationships under the same $\Delta\sigma$ and μ used in Section 2.5

Empirical relationship	Slip value (mm)			
	M_S = 1.0	M_S = 2.0	M_S = 3.0	M_S = 4.0
$\log\left(\frac{\Delta\sigma}{2\mu}M_0\right) = 16.1 + 1.5M_S$	1.81	5.74	18.15	57.39
$\log(M_0) = 16.1 + 1.5M_L$	6.62	18.33	50.79	140.69
$\log(M_0) = 17.67 + 0.905M_L$	9.53	17.62	32.58	60.25
$\log(M_0) = 9.8 + M_L$	0.026	0.05	0.10	0.20

had a short recurrence interval of approximately 140 days, but S16 had a long recurrence interval of approximately 4.2 years (1,536 days) from the first earthquake that occurred in November 2009 to the second earthquake that occurred in February 2014.

Li et al. [34] analyzed the repeated earthquakes detected in the central and northern sections of the Longmenshan fault zone and inferred that before the Wen-Chuan earthquake, the characteristics of deep sliding acceleration ("acceleration synergy") appeared in both the northern section (main earthquake source area) and the southern end (non-source area). Furthermore, the phenomenon of acceleration moment release can be judged as a mid-term precursor before strong earthquakes [35].

Similarly, we used the approximate formula $E = 10^{1.5\times M_S}$ for the relationship between the earthquake surface magnitude and energy to compute the accumulated release energy for each sequence. For the sequence, S16 (Figure 10a), before the M2.0 earthquake occurred on September 26, 2019, S16 owned an obviously accelerated release phenomenon, and 226 days later, the M5.2 earthquake occurred in the northeast direction of the location of S16. Based on sequences S08, S11, and S17 (Figure 10b), before the M6.4 earthquake occurred on January 19, 2020, the earthquake energy showed an accelerated release, and the time intervals were 1,274, 542, and 777 days, respectively. Based on sequences S18 and S20 (Figure 10c), before the M5.0 earthquake occurred on January 10, 2015, the earthquake energy release accelerated, and the time intervals were 1,036 and 280 days respectively.

According to the results mentioned in the previous paragraph, we obtained a mean time interval was approximately 690 days, and the longest time interval was approximately 1,300 days. As shown in Figure 10d, until February 2025, there will be a high major seismic risk near S06, S12, or S21.

4 Discussion

We identified 432 repeat sequences composed of 307 double lets and 125 multi-lets from a total of 19,442 events waveforms, which were recorded at nine stations along the large faults (F1–F5) in the Ka-Ping Block between September 2009 and April 2022.

Relocating the relative locations of every event in each sequence, we obtained the spatial distribution of the annual slip rate and depth distribution along the profiles, the average of the annual slip rate along F1, F2, F3, and F5 was 4.57, 4.08, and 4.89, 4.59, respectively, and the slip rates from deep were usually larger than those of the shallow ones. In addition, the slip rate in the western side of the PiQiang fault was higher than in the eastern portion, which was consistent with the GPS observations [36].

There are five asperities within the Ka-Ping Block, and they are AHQ to WUS along F1, from WUS to SMY along F2 and F3, from 90 to 150 km along F5, and from KEP station to 240 km along F5; they may be the higher seismic risk areas. Meanwhile, the locations near S16 (i.e., southwest of KEP station) and S21 (i.e., east of KEP station) will have a higher risk of moderate seismic until February 2025.

Due to the cause of the asperity, in which there are almost no repeat earthquake sequences that occur within a long time, we cannot know the urgency in time, and this is one of the limitations. The other limitation is the selection of some key parameters, which is the appropriate is very important in this study. For example, there are many empirical relationships between magnitude (M_L or M_S) and moment (M_0), such as formulas (4)–(6) [27,29,37]:

$$\log(M_0) = 16.1 + 1.5M_{L,} \tag{4}$$

$$\log(M_0) = 17.67 + 0.905M_L, \tag{5}$$

$$\log(M_0) = 9.8 + M_L. \tag{6}$$

Combining the formula (1) (in Section 2.5), we obtained the results for comparison (Table 3). According to the actual situation, formula (1) is more suitable, which is also an important reason for adoption.

Our observations of repeating earthquakes along faults have limited implications for assessing the risk of seismic hazards because of limitations such as short time periods and positioning accuracy, and the above results may not necessarily match the actual situation.

Acknowledgements: Xinjiang Seismic Station provided the waveform data, Lihua Fang provided the hypoDD code, the two anonymous reviewers proposed critical comments, and the Associate Editor significantly improved the quality of this article. We express our gratitude to the above unit or individuals and the project funds.

Funding information: This study was supported by the funding named Key R&D Program of Xinjiang Uyghur Autonomous Region (2020B03006-2, 2020B03006-3, and 2022B03001-1), Strategic Priority Research Program(B) of the Chinese Academy of Sciences (XDB18000000), National Key Research and Development Program of China (2022YFC3003703-4), National Natural Science Foundation of China (42274014, 41874015, and 41874003), and National Foreign Experts Program (G2022045013L).

Author contributions: Chaojun Gao prepared the manuscript with contributions from all co-authors. Daiqin Liu

and Jie Li are responsible for information communication, coordination, and overall arrangement. Chunyan Song carried them out for computing and organized related results. Gulizinat Yiderresi and Ailixiati Yushan Collected data and established models.

Conflict of interest: The authors have declared that no competing interests exist.

Data availability statement: Data associated with this research are confidential and cannot be released.

References

[1] Susilo A, Alamsyah MJ, Aprilia F, Hisyam F, Rohmah S, Hasan MFR. Subsurface analysis using microtremor and resistivity to determine soil vulnerability and discovery of new local fault. Civ Eng J. 2023;9(9):2286–99. doi: 10.2899/CEJ-2023-09-09-014.

[2] Guo-sheng Q, Yi-gang LI, Jie C, Bao-kun N, Yan-feng LI, Jun LI, et al. Geometry, kinematics and tectonic evolution of kepingtage thrust system. Earth Sci Fronties. 2003;10:142–52. (in Chinses).

[3] Xiao-Ping Y, Yong-kang R, Fang-min S, Xi-wei X, Jian-wu C, Wei M, et al. The Analysis for Crust Shortening of KalPin Thrust Tectonic Zone, Southwestern TianShan, Xinjiang, China. Seismol Geol. 2006;28(2):194–204. (in Chinese).

[4] Wei M, Fang-min S, Zhu-jun H, Xi-Wei X. The Preliminary Study on Paleoearthquakes Along the Western Segment of KalPinTag Fault. Seismol Geol. 2006;28(2):234–44. (in Chinese).

[5] Reigber C, Michel GW, Galas R, Angermann D, Klotz J, Chenc JY, et al. New space geodetic constraints on the distribution of deformation in central Asia. Earth Planet Sci Lett. 2001;191:157–65. doi: 10.1016/S0012-821X(01)00414-9.

[6] Densmore AL, Ellis MA, Li Y, Zhou RJ. Active tectonics of the Beichuan and Pengguan faults at the eastern margin of the Tibetan Plateau. Tectonics. 2007;26:TC4005. doi: 10.1029/2006TC001987.

[7] Geller RJ, Mueller CS. Four similar earthquakes in central California. Geophys Res Lett. 1980;7(10):821–4.

[8] Nadeau RM, Johnson LR. Seismological studies at Parkfield VI: Moment release rates and estimates of source parameters for small repeating earthquakes. Bull Seismol Soc Am. 1998;88:790–814.

[9] Hughes L, Chamberlain CJ, Townend J, Thomas AM. A repeating earthquake catalog from 2003 to 2020 for the Raukumara Peninsula, northern Hikurangi subduction margin, New Zealand. Geochem Geophys Geosyst. 2021;22:e2021GC009670. doi: 10.1029/2021GC009670.

[10] Yoshida K. The Mw 6.0–6.8 quasi-repeating earthquakes off Miyagi, Japan, with variable moment release patterns due to a hidden adjacent slip patch. J Geophys Res: Solid Earth. 2023;128:e2022JB025654. doi: 10.1029/2022JB025654.

[11] Kate HC, Ruey JR, Jyr CH. Variability of repeating earthquake behavior along the Longitudinal Valley fault zone of eastern Taiwan. J Geophys Res. 2009;114:B05306. doi: 10.1029/2007JB005518.

[12] Jiang CS, Wu ZL, Li YT, Ma TF. "Repeating Events" as Estimator of Location Precision: The China National Seismograph Network. Pure Appl Geophys. 2014;171:413–23. doi: 10.1007/s00024-012-0508-2.

[13] Nadeau RM, McEvilly TV. Fault slip rates at depth from recurrence intervals of repeating microearthquakes. Science. 1999;285:718–21. doi: 10.1126/science.285.5428.718.

[14] Li L, Chen QF, Niu FL. Repeating microearthquakes and deep deformation along the major faults in the Sichuan-Yunnan region, China. Chinese. J Geophys. 2021;64(12):4308–26(in Chinese).

[15] Dennise CT, Robert MN, Roland B. Behavior of repeating earthquake sequences in central California and the implications for subsurface fault creep. Bull Seismol Soc Am. 2008;98:52–65. doi: 10.1785/0120070026.

[16] Li L, Chen QF, Niu FL, Su JR. Deep slip rates along the Longmen Shan fault zone estimated from repeating microearthquakes. J Geophys Res. 2011;116:B09310. doi: 10.1029/2011JB008406.

[17] Ran YK, Yang XP, Xu XW, Chen LC. Deformation pattern and short Tening rates in the east part of Kaping thrust system in southwest Tian-Shan during late quaternary. Seismol Geol. 2006;28:179–93. (in Chinese).

[18] Menke W, Lerner-Lam AL, Dubendorff B. Polarization and coherence of 5 to 30 Hz seismic wave fields at a hard-rock site and their relevance to velocity heterogeneities in the crust. Bull Seismol Soc Am. 1990;80:430–49.

[19] Menke W. Using waveform similarity to constrain earthquake locations. Bull Seismol Soc Am. 1999;89:1143–6.

[20] Schaff DP, Richards PG. Repeating seismic events in China. Science. 2004;303:1176–8.

[21] Schaff DP, Richards PG. On finding and using repeating seismic events in and near China. J Geophys Res. 2011;116:B03309. doi: 10.1029/2010JB007895.

[22] Han LB, Wu ZL, Li YT, Jiang CS. Cross-correlation coefficients for the study of repeating earthquakes: An investigation of two empirical assumptions/conventions in seismological interpretation practice. Pure Appl Geophys. 2014;171:425–37. doi: 10.1007/s00024-012-0515-3.

[23] Li B, Li X. Study on the test error of silt dynamic Characteristic and Its Influence on the Peak Ground Acceleration. HighTech Innov J. 2023;4(1):64–74. doi: 10.28991/HIJ-2023-04-01-05.

[24] Wu SC, Cornell CA, Winterstein SR. A hybrid recurrence model and its implication on seismic hazard results. Bull Seismol Soc Am. 1995;85:1–16. doi: 10.1785/BSSA0850010001.

[25] Li L, Chen QF, Cheng X, Niu FL. Spatial clustering and repeating of seismic events observed along the 1976 Tangshan fault, north China. Geophys Res Lett. 2007;34:L23309. doi: 10.1029/2007GL031594.

[26] Cheng XF, Niu PG, Silver S, Horiuchi K, Takai YL, Hisao I. Similar microearthquakes observed in western Nagano, Japan, and implications for rupture mechanics. J Geophys Res. 2007;112:B04306. doi: 10.1029/2006JB004416.

[27] Hanks TC, Kanamori H. A moment magnitude scale. J Geophys Res. 1979;84:2348–50. doi: 10.1029/JB084iB05p02348.

[28] Kanamori H, Anderson DL. Theoretical basis for some empirical relations in seismology. Bull Seismol Soc Am. 1975;65:1073–95.

[29] Pan Zhen-sheng LH, Gu Mei-jiu L-D, Qi S. Preliminary Study on Source Parameters of Earthquakes Occurred in Keping Block, Xinjiang. Seismol Res Lett. 2010;32(4):357–410. (in Chinese).

[30] Waldhauser F, Ellsworth WL. A double-difference earthquake location algorithm: Method and application to the northern Hayward fault, California. Bull Seismol Soc Am. 2000;90:1353–68. doi: 10.1785/0120000006.
[31] Nadeau RM, McEvilly TV. Fault slip rates at depth from recurrence intervals of repeating microearthquakes. Science. 1999;285:718–21. doi: 10.1126/science.285.5428.718.
[32] Igarashi T, Matsuzawa T, Hasegawa A. Repeating earthquakes and interplate aseismic slip in the northeastern Japan subduction zone. J Geophys Res. 2003;108(B5):2249. doi: 10.1029/2002JB001920.
[33] Rau RJ, Chen KH, Ching KE. Repeating earthquakes and seismic potential along the northern Longitudinal Valley fault of eastern Taiwan. Geophys Res Lett. 2007;34:L24301. doi: 10.1029/2007GL031622.
[34] Li L, Chen QF, Niu FL. Repeating microearthquakes and deep deformation along the major faults in the SichuanYunnan region. Chin J Geophysics. 2021;64:4308–26 (in Chinese).
[35] Jiang CS, Wu ZL. Accelerating moment release (AMR) before strong earthquakes: A retrospective case study of a controversial precursor. Chin J Geophysics. 2009;52:691–702 (in Chinese).
[36] Li J, Yao Y, Li R, Yusan S, Li G, Freymueller JT, Wang Q. Present-day strike-slip faulting and thrusting of the Kepingtage fold and-thrust belt in southern Tianshan: Constraints from GPS observations. Geophys Res Lett. 2022;49:e2022GL099105. doi: 10.1029/2022GL099105.
[37] Abercrombie RE. The magnitude-frequency distribution of earthequakes recored with deep seismometer at Cajon Pass, southern California. Tectonophysics. 1996;261:1–7. doi: 10.1016/0040-1951(96)00052-2.